International Journal of Engineering Materials and Manufacture (2023) 8(3) 51-66
https://doi.org/10.26776/ijemm.08.03.2023.01

Failure Investigation on Failed Towing Arm of an Aircraft: A Case of Improper Material Processing and Failed Repair Welding of a Cast Al-Cu-Si Type Aluminium Alloy

Mrityunjoy Hazra and Ashok Kumar Singh

Received: 01 March 2023
Accepted: 19 May 2023
Published: 01 July 2023
Publisher: Deer Hill Publications

ABSTRACT
Present work describes the metallurgical failure investigation of a failed towing arm/bar. Aircraft attached with this incident travelled a distance of 2 km with normal towing speed (8 km/hr). The component is said to have broken while turning to right from taxi track and then turning left about 15-20°. The mating fracture pieces of the failed towing arm fork along with bent towing pin were analyzed for failure investigation. Parent material of the towing arm has been found to be a cast Al-Cu-Si alloy closely matching with the alloy 295 used in T6 condition. Pin is made of mild steel. Failure of the towing arm fork has been initiated by weld solidification cracking of the weld region at close to the fusion line. Liquation cracks at heat affected zone (HAZ) have aggravated the situation further by weakening the microstructure and facilitating the crack propagation. Grain boundary precipitates of Al-Cu-Fe type in HAZ have facilitated the propagation of failure along with the liquation cracking. On the other hand, Al-Fe-Mn type of precipitates sitting along the grain boundaries in weld area seems to have not facilitated the failure initiation unlike the solidification cracking. Improper material processing has led to the weakening of the bulk microstructure and thus the component itself, by introduction of various defects (pores, grain fall out, thick Al-Cu-Fe type of continuous grain-boundary precipitates and cracking). Weld repairing has been found to be a failure in Al-Cu-Si system in the present component.
Keywords: Towing arm, cast Al-Cu-Si, repair welding, hot cracking, solidification cracking, liquation cracking, intergranular fracture, Al-Cu-Fe grain boundary precipitates, Al-Fe-Mn grain boundary precipitates.

1 INTRODUCTION
1.1 Background Information
Generally, aircrafts are shifted from Hanger to Pan (operational parking area / shelters provided by the sites of the runway) by towing process. The towing distance depends on the locations of Hanger and Pan. The towing bar broke while turning to right from taxi track and then turning left about 15-20°. The towing distance for this particular case is about 2 km. In further examination, it has been observed that the left side of the towing bar fork end broke during towing process on a normal track i.e., without significant slope from taxi track to Pan. The aircraft towed almost 2 km and towing speed was normal about 8 km/hr. The mating fracture pieces of the failed towing arm fork along with bent towing pin were analyzed for failure investigation, while towing spool (part of aircraft which is attached with towing arm for pulling it along with tractor) was found to be intact (undamaged) and likewise not destroyed for analysis. Present paper is thus concerned with the failure investigation of the failed towing arm fork along with bent towing pin.

1.2 Literature Review
Towing is a method of movement of large aircraft about the airport, flight line and hangar without use of engine power of an aircraft [1]. It is commonly carried out by towing with a tow tractor or tug. Hand pushing on the correct areas of the aircraft may be helpful in the case of the small aircraft. Certain qualified personnel are also sometimes permitted for taxiing the aircraft about the flight line. Reckless or careless duty on towing an aircraft may cause hazard, resulting in damage to the aircraft and importantly injury to the personnel. Thus, the specific instructions for each model of aircraft as prescribed in the manufacturer's maintenance manual must be followed. A qualified person

M. Hazra ✉, A. K. Singh
Defence Metallurgical Research Laboratory (DMRL)P.O. Kanchanbagh, Hyderabad 500 058, India
E-mail: mhazra@dmrl.drdo.in

Reference: Hazra and Singh (2023). Failure Investigation on Failed Towing Arm of An Aircraft: A Case of Improper Material Processing and Failed Repair Welding of a Cast Al-Cu-Si Type Aluminium Alloy. International Journal of Engineering Materials and Manufacture, 8(3), 51-66.

is usually within the flight (before the flight is being moved for towing) deck to operate the brakes in case the tow bar fails or becomes unhooked. Prevention of possible damage of the aircraft can then be reduced.

Various types of tow bars available for general use are by and large utilized for towing operations of different types. Some special types of bars may be employed on a particular aircraft only. Such types are built by the aircraft manufacturer. Obtaining a sufficient tensile strength value to pull most aircraft has traditionally been the principal design criteria for these bars and very importantly, torsional or twisting loads are not intended at all. A schematic diagram of tow bar assembly is shown in Fig. 1.

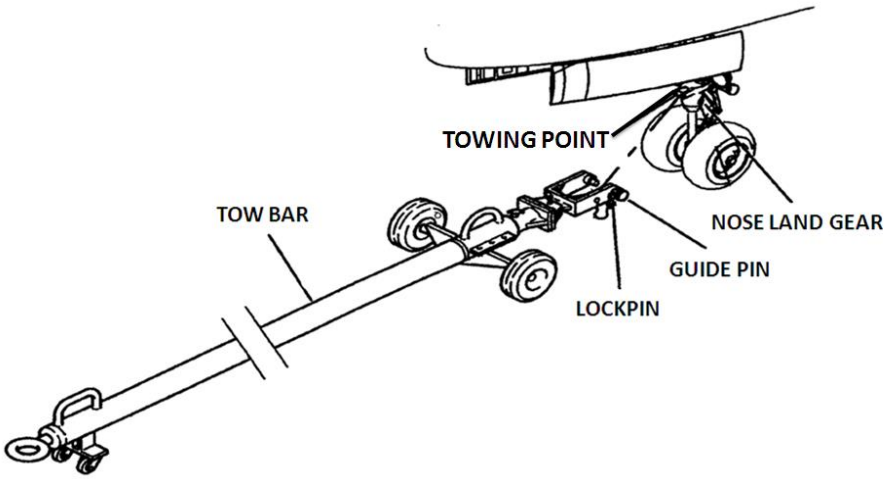

Figure 1: Schematic diagram of a tow bar assembly

Two incidents of failures of towing bars in aircraft towing system (ATS) have been reported in open literature, although with insignificant metallurgical input [2, 3]. In one case, shear pin broke and caused the failure of the whole system in airbus 319 [2]. In another case, shear bolt along with tow bar body broke in case of a Boeing 707 aircraft [3]. Fatigue mechanism has been attributed to be the cause of failure. Usually, breakage of a tow bar is not a big issue to deal with. One has to replace the tow bar and a few minutes later the aircraft would be back on its way. However, it may have sometimes, secondary damaging effect (i.e. damage caused by the failure of tow bars) which may delay the flight schedule related activities significantly. One such incident of failure of a nose gear is reported as a result of failure of tow bars (would be referred as towing arms, heretofore) [4].

2 EXPERIMENTAL PROCEDURE

Both the failed towing arm fork and bent towing pin were at first visually examined with the help of naked eye and magnifying glass. Photographs were taken in as-received condition from various orientations and preserved for future reference during the course of analysis. One of the mating fracture surfaces (dislodged piece) was extracted delicately without damaging the surface for further in-depth examination under scanning electron microscope (SEM) equipped with electron dispersive spectroscopy (EDS). The fracture surface was examined under SEM after cleaning with acetone in an ultrasonic cleaner. Subsequently, a representative cross-sectional sample was extracted from failed parts for detailed metallographic investigation. The broken piece of towing arm fork was sectioned into three parts across the thickness. It was done very delicately with the sequence of cold mounting followed by sectioning through slow speed isomet cutter. The polished sample surfaces were examined under optical microscope and SEM.

The bent portion of the towing pin was prepared for metallographic study in both the un-etched and etched conditions. Keller's reagent was used for etching the towing arm fork pieces, while 2 % nital was employed as etchant for towing pin. Bulk compositional analysis of the failed components was carried out by X-ray florescence spectroscopy (XRF) and EDS techniques followed by verification of results with those obtained from inductively coupled plasma optical emission spectroscopy (ICP-OES). Vickers hardness readings were taken at 5 kg load on metallographically prepared samples.

3 RESULTS

3.1 Visual Examination

As-received failed components are shown in Fig. 2. Fractured towing arm fork end bent towing pin along with intact (undamaged) towing spool are seen. Red colour paint is seen to cover the entire towing arm fork. Fig. 3 reflects fracture surfaces of towing arm fork end in various views. Typical brittle fracture of as-cast products seems to prevail, as is typified by coarseness of the fracture features. There is existence of well revealed weld regions in the surroundings of the fracture surfaces. Probable detached/peeled off parts during service which seem to have been welded later on have been marked (Fig. 3(d, e and f)). These are quite easily identifiable by visibly clear weld beads (boxed). Clear visibility is obvious for weld region, base material as well as the heat-affected zone (HAZ) on the failed surfaces (Fig. 3 (a, b and c)). A prominent secondary crack spanning across the whole fracture surface and almost at boundary

(fusion line) between the weld region and the rest of the cross-section (consisting of HAZ and base material) is seen (Fig. 3 (b and c)). Also, the mating failed surface reveals some small secondary cracks at the welds close to the boundaries of weld and HAZ in two perpendicular sides (in 2-dimension) of the failed component (Fig. 3g). These cracks are along the weld-HAZ boundary at one side weld as well. Henceforth, weld regions with bigger and smaller dimensions at two perpendicular directions are referred as longitudinal and transverse welds, respectively. The counterpart of the fracture surface presented in Fig. 3a is shown in Fig. 3h. This is a magnified view of high resolution of the portion presented in Fig. 3b. Here, one may notice the disparity between weld thicknesses in longitudinal and transverse welds.

3.2 Fractography

Fractographs are presented in Figs. 4-7 along with EDS analyses. Intergranular fracture features have been found to be prevalent. Fig. 4 displays low magnification image showing intergranularity of the fracture surfaces. Figs. 4 and 5 (a, b and c) represent fracture features from HAZ (marked in Fig. 3b). On the other hand, representation of weld fracture is in Fig. 5d. Summary of all the types of fracture features observed at various locations on the surface is presented in Fig. 5. Gas-hole and/or porosity have been observed occasionally (boxed region in Fig. 5a). Intergranular fracture features is quite noticeable along with shallow rubbing. Deep secondary cracks along the intergranular channels have been observed (Fig. 5 (c and d)). Interestingly, this fracture feature also resembles the appearance of pores (Fig. 5c). It is to be noted that the type of intergranularity differs in features presented in Fig. 5(b and c) to Fig.5d. Signature of cleavage within the intergranular fractures has also been noticed occasionally (Fig. 5 (c and d)). Intergranularity in fracture is more vivid in a location presented in Fig. 5d, in contrast to the rubbed intergranular fracture of the few other locations observed in Fig. 5c.

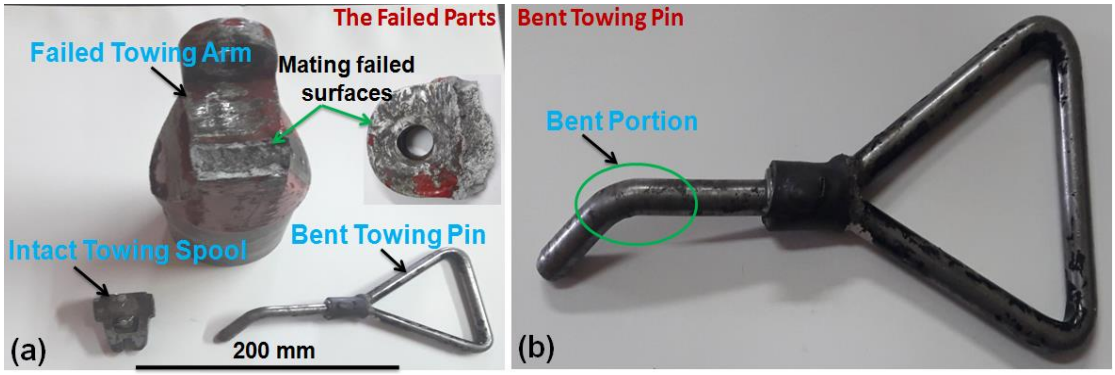

Figure 2: Photographs of the as-received broken towing arm fork and bent towing pin

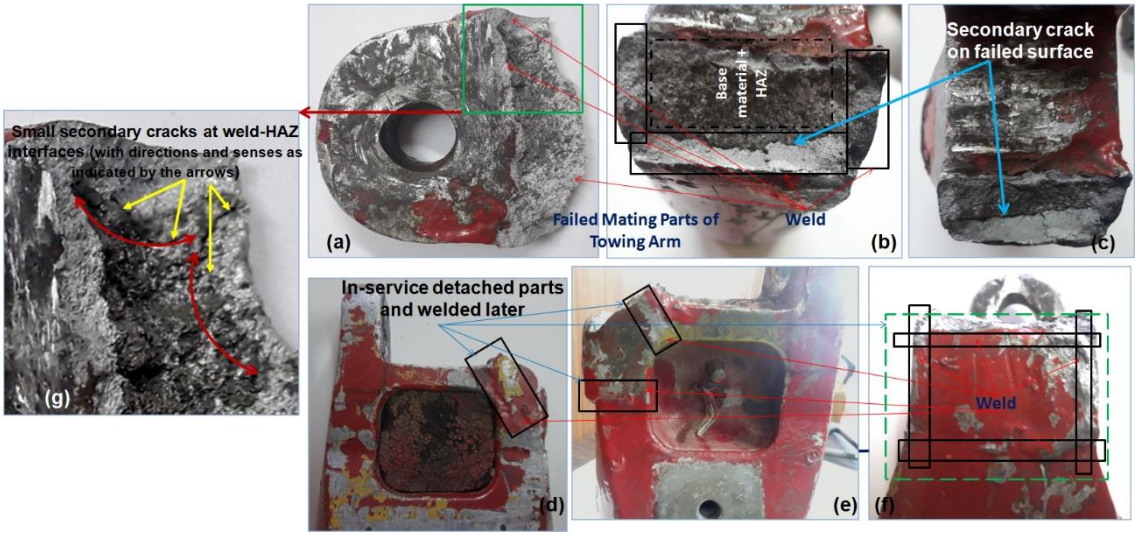

Figure 3: Photographs of fracture surfaces of towing arm fork end in various views

EDS analysis on the location marked as 1 (Fig. 5b) reveals the presence of Al and O majorly (Fig. 6). It basically reflects the composition of the tiny round particles present in that location. Fractographs near the weld region (along one of the side welds) are shown in Fig. 7. Again, HAZ in this region reflects intergranular fracture, while fracture of the weld zone is completely cleavage type. However, intergranular channels are even quite visible within this cleaved surface. Very prominent secondary crack has also been observed at the boundary or interface between the weld zone and HAZ.

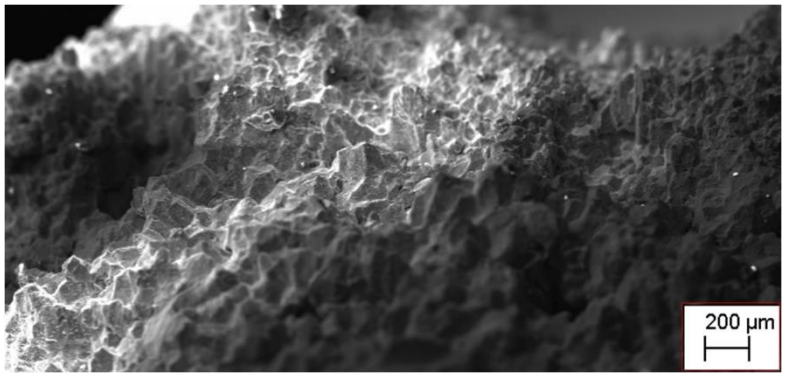

Figure 4: Low magnification SEM image of fracture surface

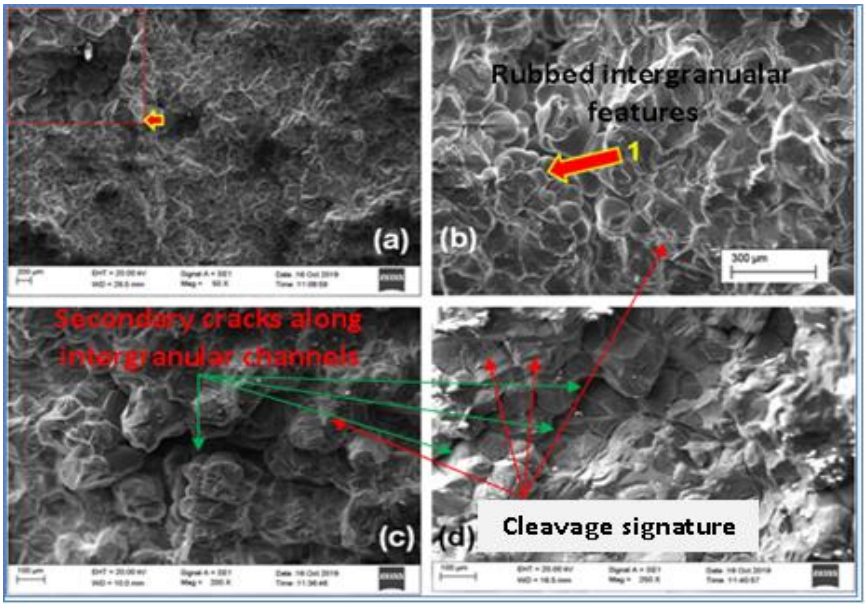

Figure 5: Summarized view of the various types of fractures observed in the present failure

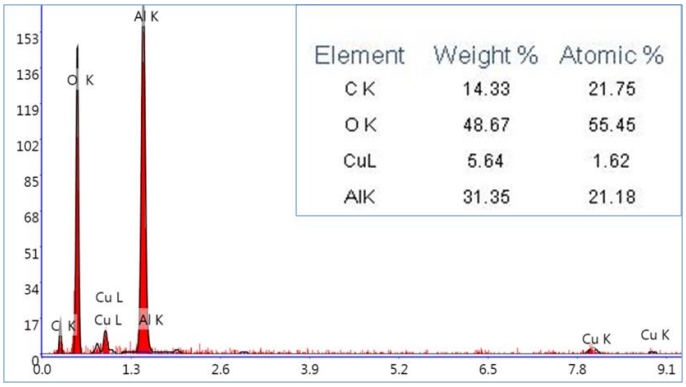

Figure 6: EDS analysis pattern taken on location 1 (Fig. 5b)

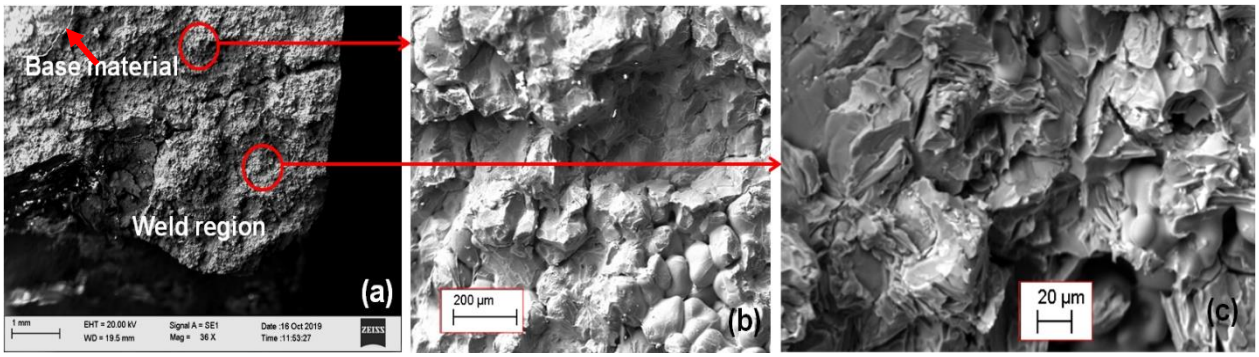

Figure 7: Fractographs near the weld region

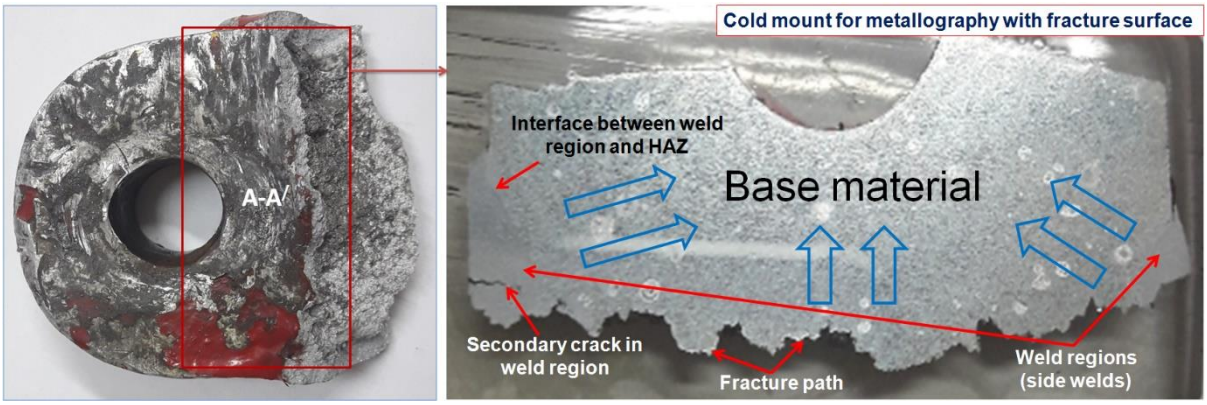

Figure 8: Cold mount containing towing arm fractured end along with location of the sample in main fractured piece

3.3 Metallography

Towing arm fork (henceforth, it will be referred to as towing arm only) fractured section mounted in cold mount along with the schematic view of the location of the sample in main fractured piece is shown in Fig. 8. Existence of weld regions at two sides or edges is very clear. This image may be seen along with the as-received photographs presented in Fig. 3(a, d-f), so as to have quite a good idea about the relative location of the weld, HAZ and base material within the fractured component. It has also been found to contain secondary cracks intermittently, as one such is marked in Fig. 8b. It is to be noted that the crack trajectory and orientation of secondary cracks is exactly matching with the fracture path (main crack causing the fracture) (Fig. 8). Grain boundary precipitates and occasional cracking along these precipitates have been observed throughout the base as well as weld region in the un-etched condition (Fig. 9).

Microstructure exhibits the presence of well revealed weld zone and base material after etching (Fig. 10). Weld region contains few dendrites with 90° angle between primary and secondary dendritic arms indicating that the weld material is cubic. Interestingly, both the heat affected zone (HAZ) and remaining base material reveal the presence of equiaxed grains. Heat-affected zone (HAZ) of a spread of 0.7 mm has been found and contains numerous cracks and grain fallouts (Fig. 10). Low magnification SEM images are shown in Fig. 11. Ample of pores has been found in both the regions, i.e., weld as well as base material. Amount of pores seems to have been more in weld than that in the base material. High magnification images of the weld region and base material are presented in Fig. 12(a, b) and Fig. 12(c-e), respectively. Again, area fraction of the cracks is found to be more in case of weld region than that in the base material.

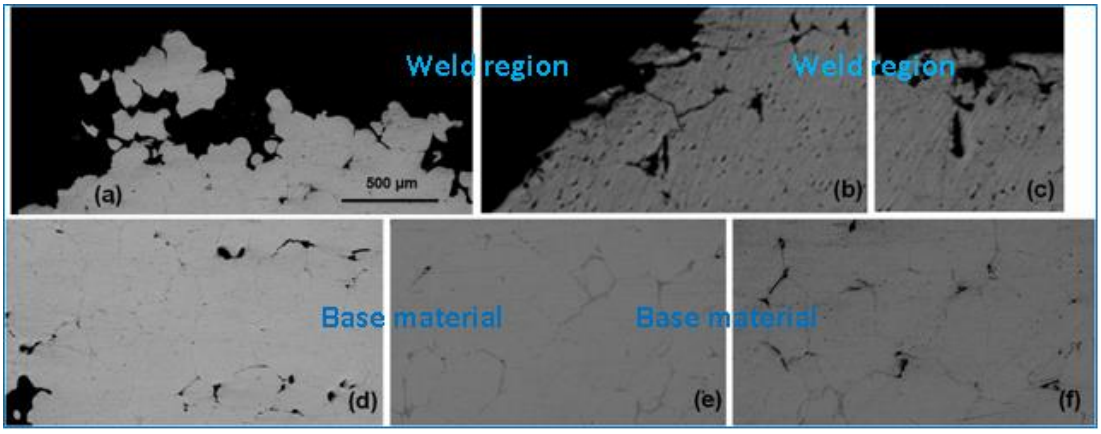

Figure 9: Optical microstructures of the failed towing arm end in un-etched condition

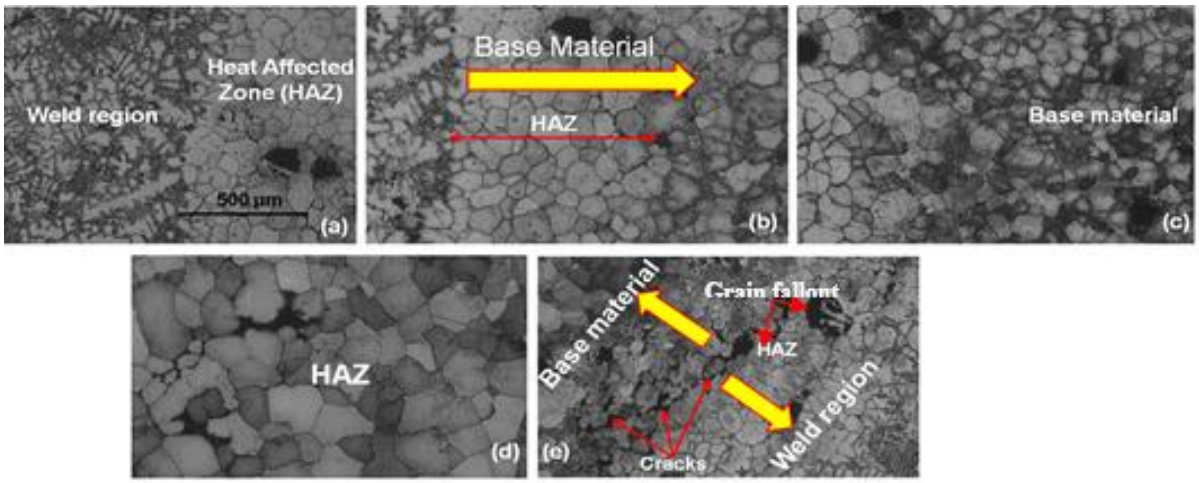

Figure 10: Optical microstructures of the towing arm end in etched condition

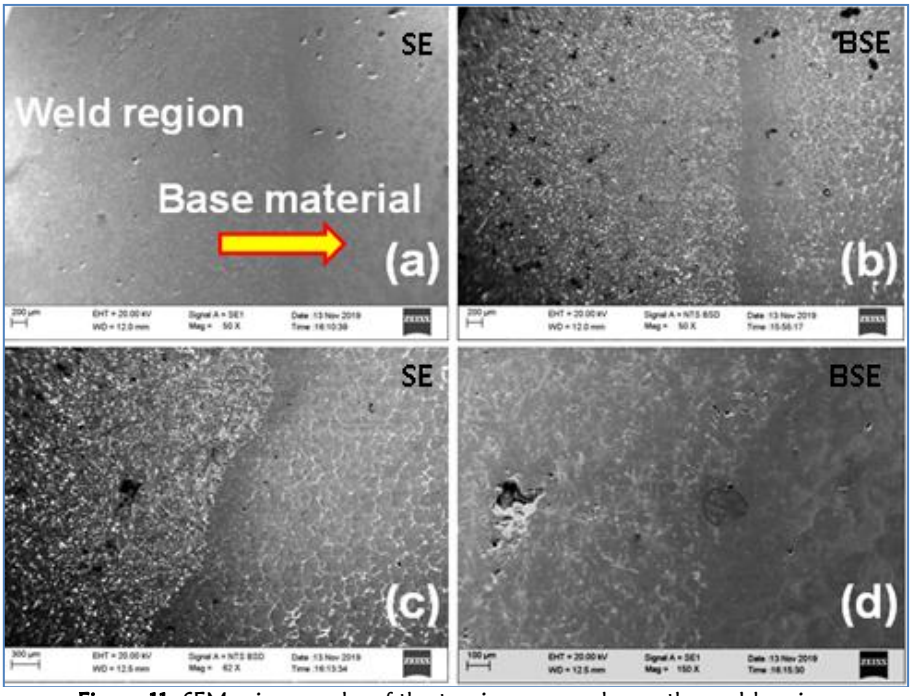

Figure 11: SEM micrographs of the towing arm end near the weld region

The EDS analyses on various phases in the weld zone are presented in Fig. 13. Some precipitates appear to reside along the grain boundaries have been found to be rich in Al, Fe and Mn. Eutectic phases contain mainly Al and Si. Overall composition of the weld region has been found to be rich in Si and Al (Fig. 14). Base material reveals the presence of grain boundaries rich in Cu, Fe and Al (Fig. 15). Defect portions of the grain boundaries contain Si, Cu along with Cl and O (Fig. 16). Overall base material composition shows the presence Al along with small amount of Cu (Fig. 17).

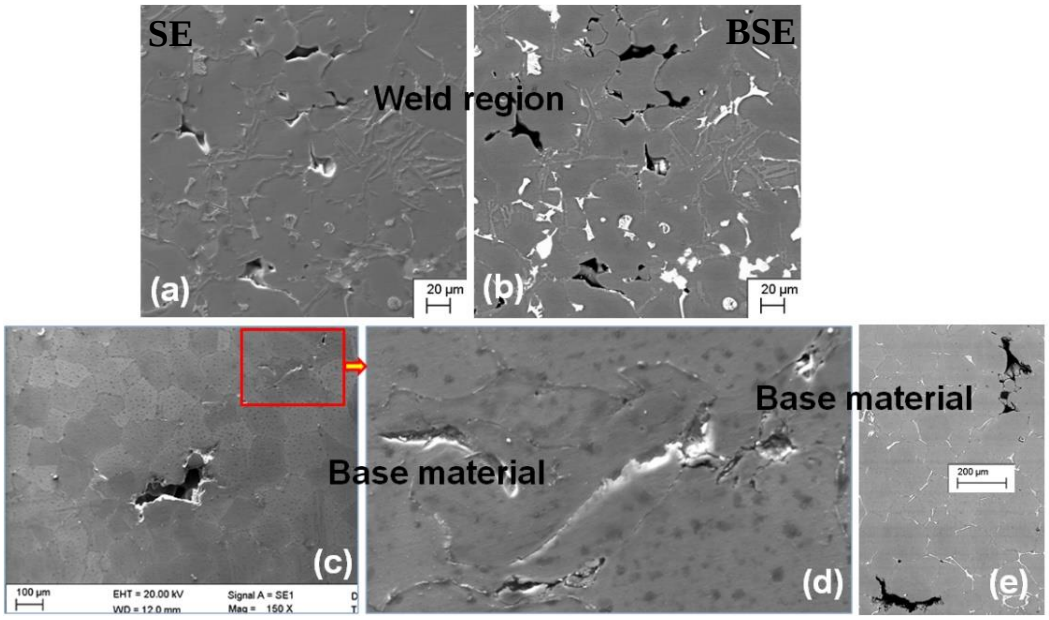

Figure 12: High magnification SEM images of the weld region and base material

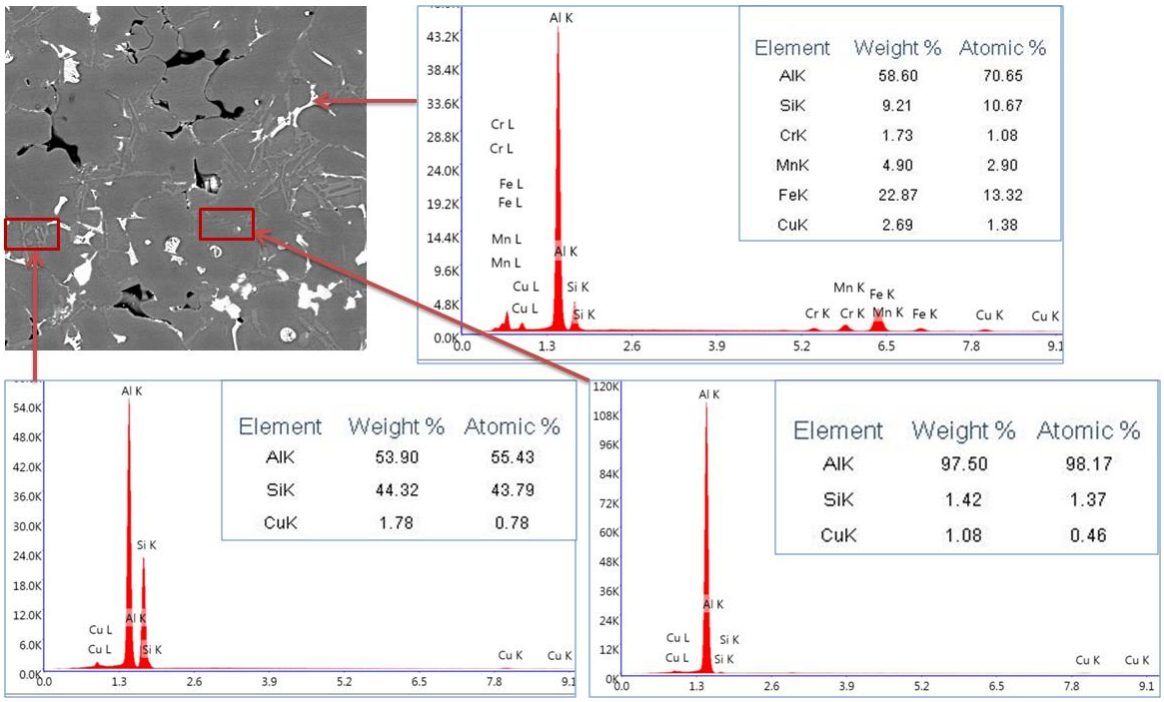

Figure 13: EDS analysis patterns on various phases in the weld zone

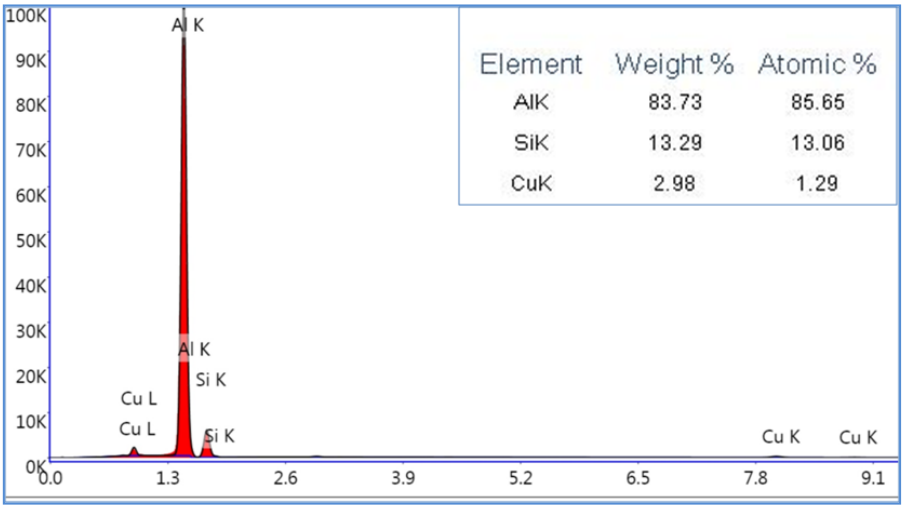

Figure 14: Overall composition of the weld region as obtained by EDS analysis

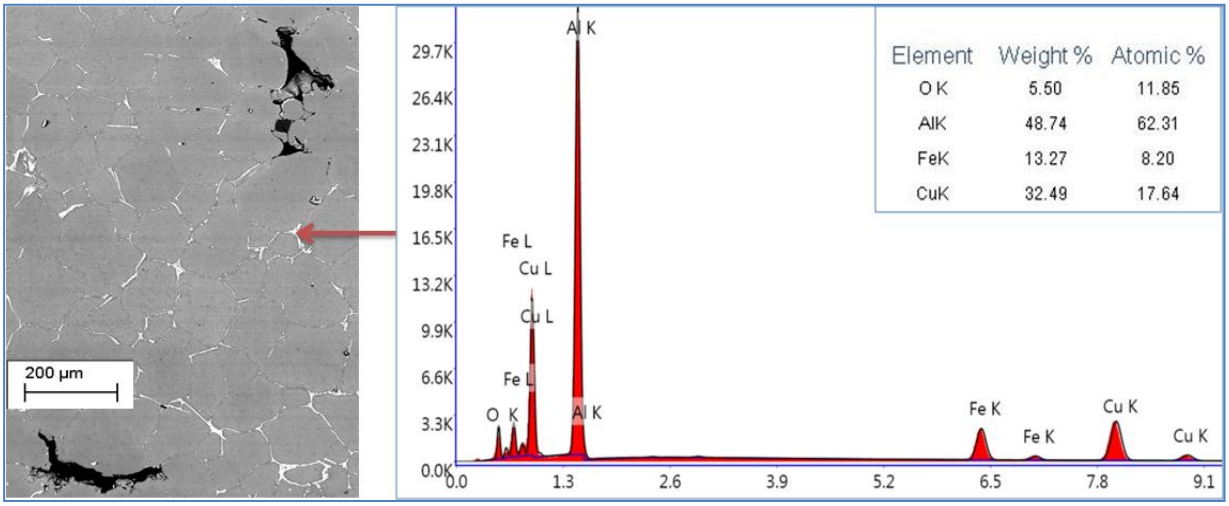

Figure 15: EDS analysis on grain boundaries in base material

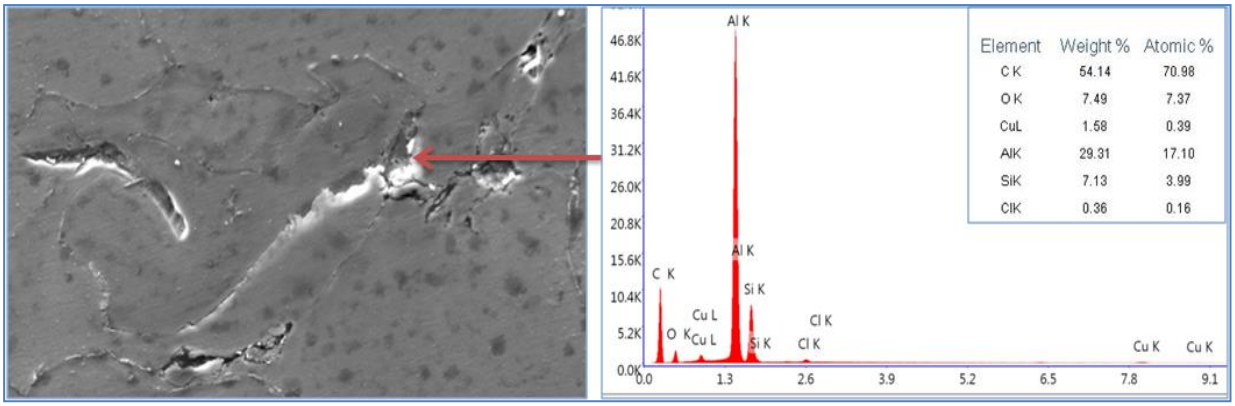

Figure 16: EDS analysis of defects on grain boundaries in base material

Fig. 18 exhibits SEM micrographs of various locations of the towing arm end away from the failed region. Reference image of sample extraction is displayed in Fig. 18(a, b). Presence of thick and continuous grain boundary precipitates are quite well revealed in the BSE images (Fig. 18(d, g)). Several microstructural defects related to grain boundary cracking and grain pullout have been observed. Fig. 19 exhibits high magnification image of the said region. Two types of precipitates have been observed: (i) rich in Cu and Fe and (ii) rich in Cu only. Matrix composition has been found to be Al containing ~ 5 wt.% Cu.

Microstructures of the towing pin are shown in Fig. 20. It reveals the presence of alternate layer of greyish and whitish phases. Three different locations marked as 1 (bright contrast), 2 (grey contrast) and 3 (overall composition) have been analyzed for composition. The EDS analysis reveals the presence of Fe only in all the three locations (Fig. 21).

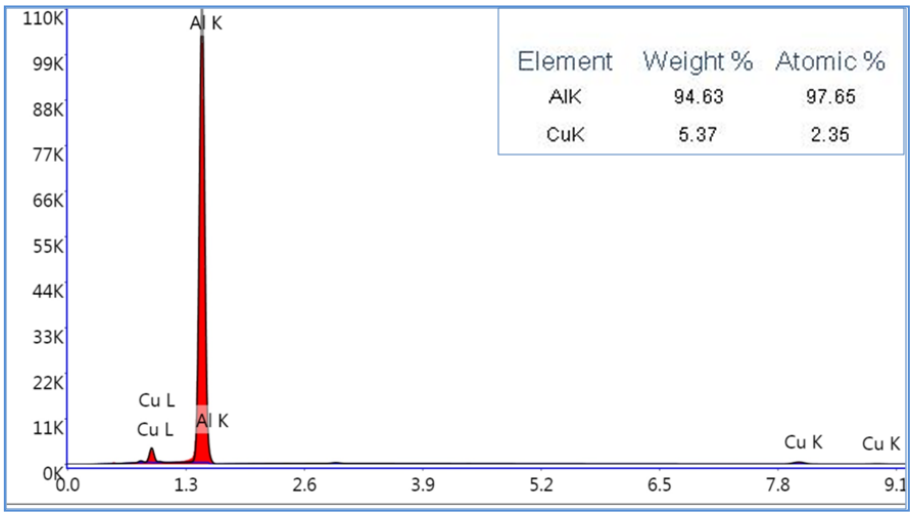

Figure 17: Overall base material composition as obtained by EDS analysis

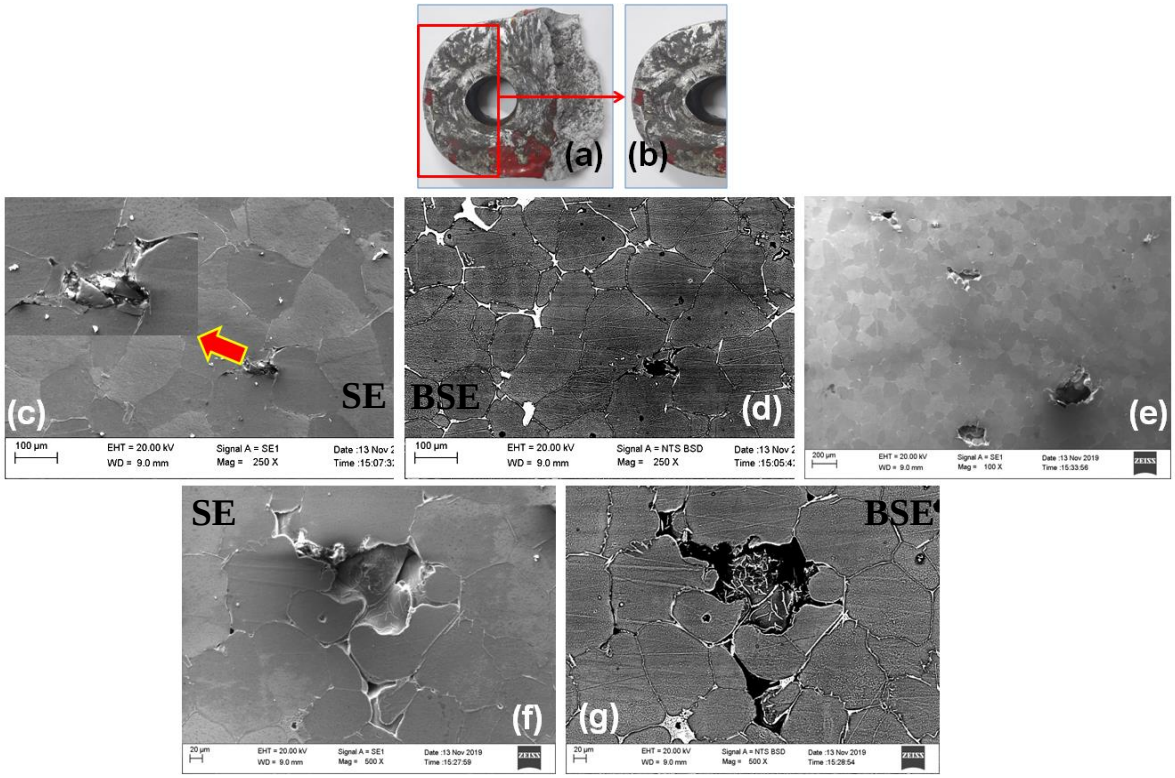

Figure 18: SEM micrographs of various locations of the towing arm end away from the failed region

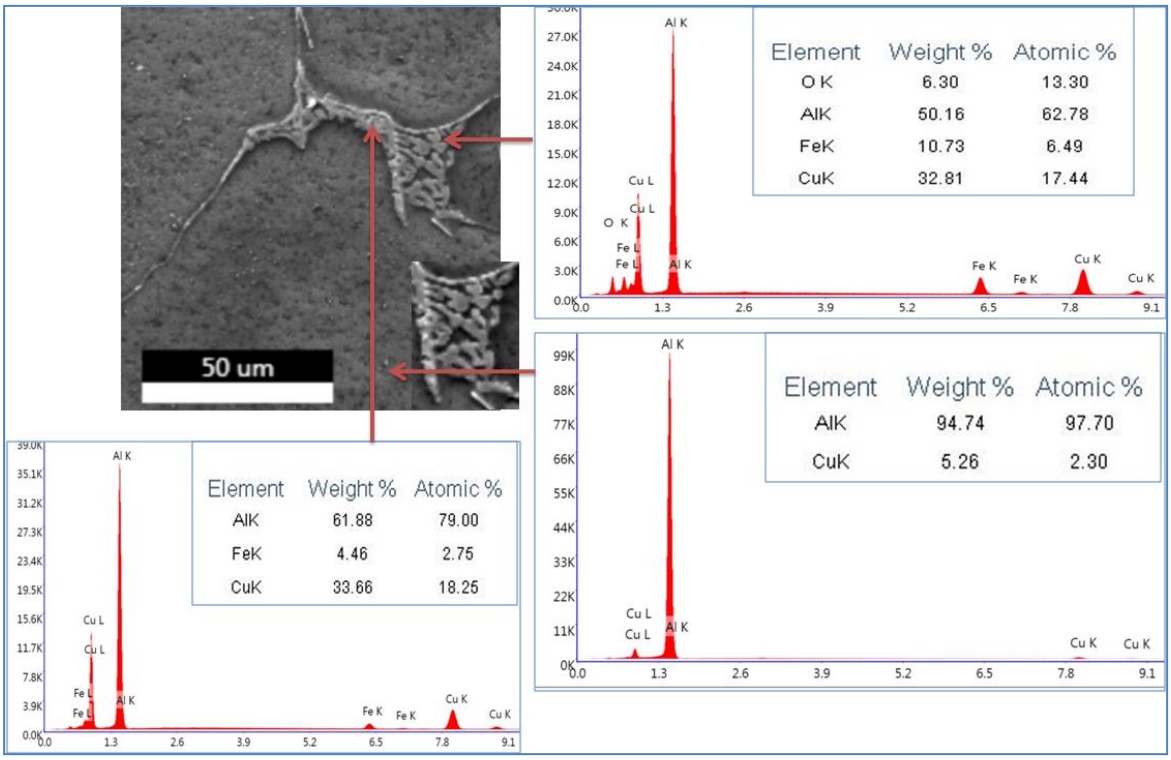

Figure 19: High magnification image along with EDS analysis on regions (Fig. 18)

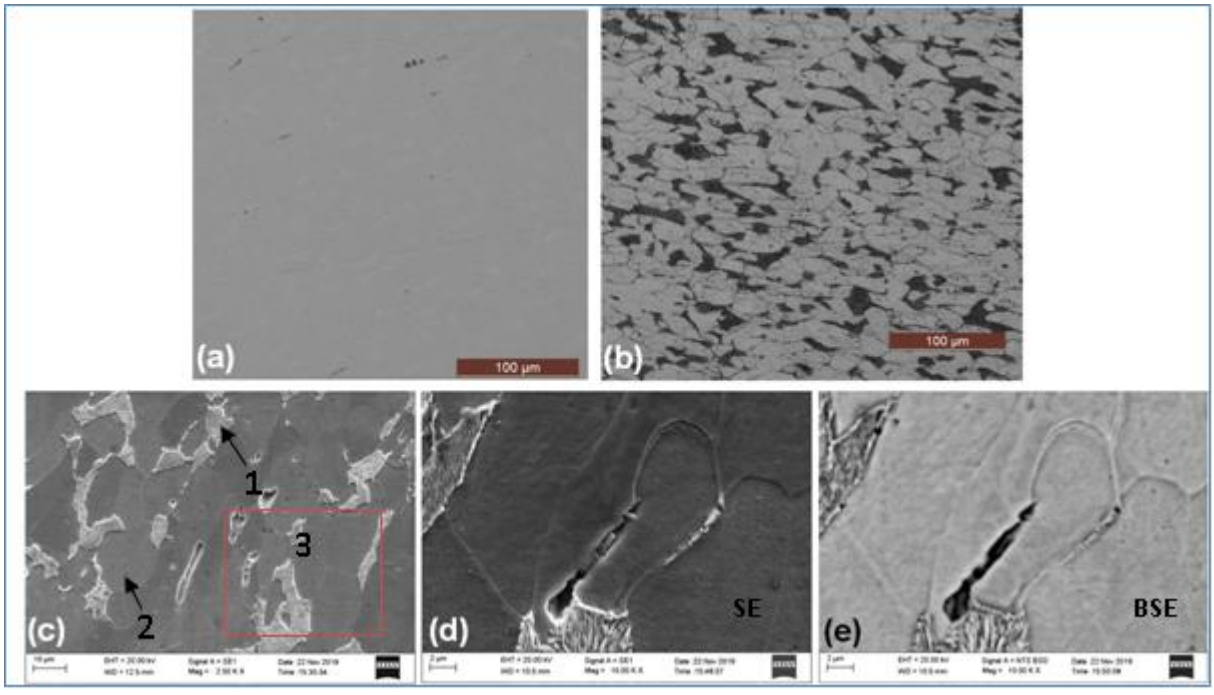

Figure 20: Optical (a, b) and SEM micrographs (c-e) of towing pin

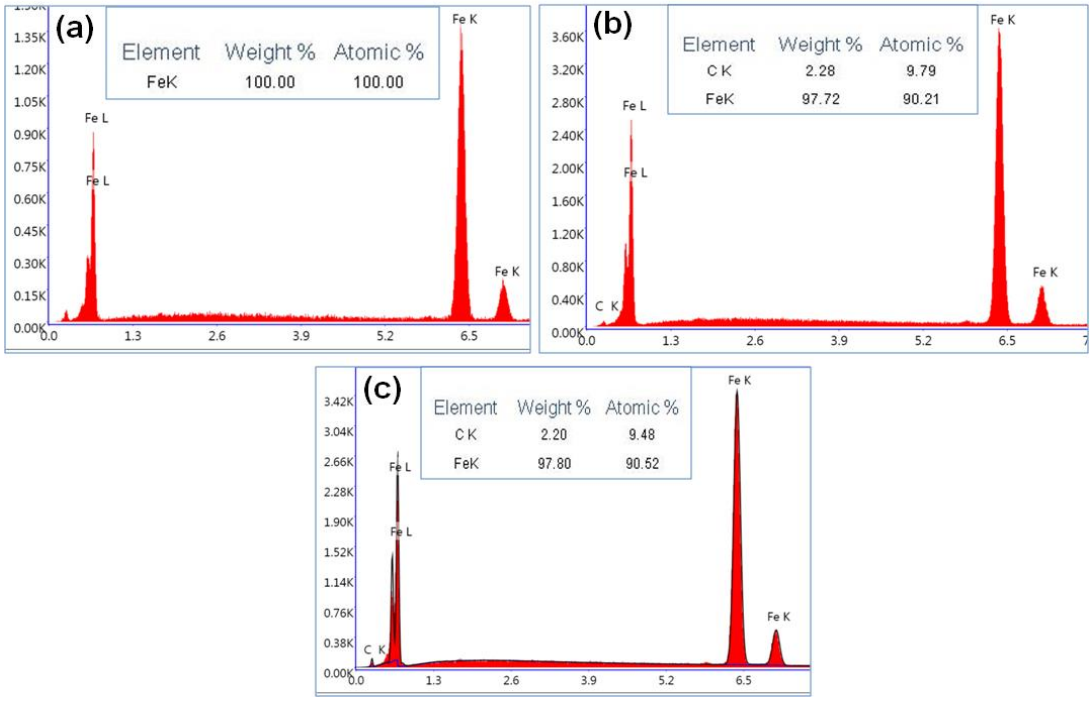

Figure 21: EDS analysis patterns on various marked locations 1, 2 and 3 (Fig. 20)

3.5 Chemical Composition

Composition of towing arm as obtained by XRF is given in Table 1. It shows Cu as the major alloying element apart from the base material Al. Towing pin is found to contain only Fe, while the EDS analysis was taken from bulk of the sample at low magnification. Compositions of the towing arm and towing pin as obtained from ICP-OES analysis is presented in Table 2. Towing arm is found to contain Cu and Si as major alloying elements along with the base Al. The analysed composition of towing arm is very close to the alloy B295 [5]. The ranges of the alloying elements in alloy B295 is included in Table 2 for ready reference. Towing pin consists of Mn as the major alloying elements along with the base Fe. Contents of the trace elements (C and S) of the towing pin are shown in Table 3.

Table 1: Chemical compositions of failed towing arm and towing pin as obtained by XRF and EDS techniques.

Component	Technique	Elements (wt.%)						
		Cu	C	Si	Ti	Ni	Fe	Al
Towing arm	XRF	4.65	-	0.35	0.15	0.009	0.132	Bal.
Towing pin	EDS	-	2.2	-	-	-	97.8	-

Table 2: Chemical compositions of the failed towing arm and towing pin obtained by ICP-OES technique

Component	Elements, wt% (Standard deviation, wt%)							
	Fe	Ni	Cu	Si	Ti	Mn	P	Al
Towing Arm	0.17 (0.01)	<0.002	4.3 (0.1)	1.03 (0.06)	0.13 (0.05)	-	-	Bal.
B295 [5]	Max. 1.0		4.0-5.0	0.7-1.5	Max.0.25	Max.0.35		Bal.
Towing Pin	Bal.	-	-	0.58 (0.06)	-	0.82 (0.06)	0.037 (0.003)	-

Table 3: Contents of trace elements (C and S) of the failed towing pin

Elements	C	S
wt.% (Standard deviation)	0.19 (0.01)	0.034 (0.002)

3.4 Hardness

Vickers hardness values of towing arm sample taken at 5 kg load are found to be 88, 102, 108, 98, 92, with an average value of 98 Hv. The weld region of Towing arm possesses hardness values (taken at 500 g load) of 103.6, 99.1, 94.2, 104.2, with an average value of 100 Hv. Towing pin possessed hardness value of 230 Hv.

A micro hardness profile taken along a line across the weld interface and covering both base and weld materials has been shown in Fig. 22. Fig. 23 is the reference image for the indentations taken on the sample. Here, one can notice that the weld material possesses an average hardness value of 102 Hv, while the same for base material is 116 Hv. It may be noted that these values are not in agreement with the bulk Vickers hardness values of the two regions as mentioned above.

Hardness value of the interface (measured on the actual interfacial line) is found to be around 100 Hv. The hardness value on the weld side ranges from 65 to 130 Hv and gets stabilized at around 2.25 mm (2250 μm) from the interface. On the other hand, hardness value spanned from 115 Hv to 125 Hv on the base metal side and gets stabilized at around only 1.5 mm (1500 μm) from the interface.

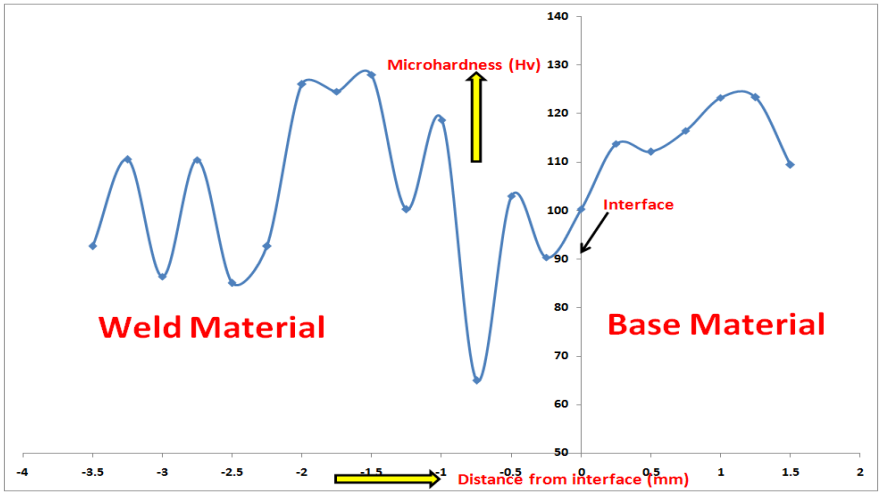

Figure 22: Micro hardness survey (in Vickers scale) across the weld interface

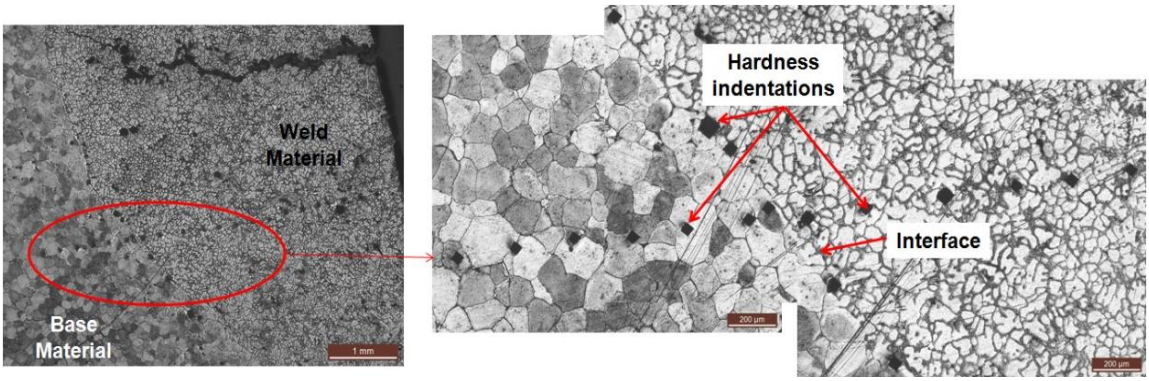

Figure 23: Reference image for the micro hardness survey across the weld interface

4 DISCUSSIONS

4.1 Material of Construction: Identity and Suitability

Microstructure, chemical composition and hardness evaluations of the as-received failed components indicate that the material of construction of towing arm is a cast Al-Cu-Si alloy (closely matching with B295 alloy in T6 condition), while that of the towing pin is a low carbon (mild) steel [5, 6]. Microstructure of the base material consists of α-Al (with Cu) along with grain boundary precipitates rich in Al, Fe and Cu and closely matching with Al_2FeCu type. The material contains defects such as pores and grain fall outs etc. quite extensively throughout its microstructure. The choice of the material composition and (casting) process route appear to be usual for the fabrication of towing arm wherein requirement of high strength, appreciable amount of ductility at room and elevated temperatures, sufficient corrosion resistance along with the involvement of extensive wear and tear is there in service [5-10].

4.2 Repair Welding: Its Presence, Need and Impact upon the Present System

There are well-defined weld regions around the circumference of the fracture surface of Towing arm. This is supported by the visual examinations as well as observation under SEM. Overall compositions of the base and weld materials as obtained from the EDS analysis reflects the use of an Al-Si base filler metal in the welding process [5, 7, 8, 11-13]. Similar level of hardness values along with gross similarity in microstructure between base and weld materials in the failed component indicate that the T6 heat treatment has been given to the component after welding.

It seems that the repair welding has been carried out to refurbish prior localized failed and detached areas (Fig. 3a). However, one must notice that the inherent defects in the base material in present case are the cracks along the grain boundary precipitates in addition to the pores and grain fallouts. Thus, the avoidance of recurrence of such failure by repair welding is not possible, unless it changes the local thermal and/or chemical history to the desired extent [13-17]. Intended microstructure resulting from this proposed change in local thermal and/or chemical history may find usefulness in such case. However, no such desired changes have been observed in present case, after the T6 heat treatment given to the whole assembly (base material + weld). Interestingly, weld material has been found to contain more defects in terms of pores and cracks than the base. Therefore, adoption of the method of repair welding does not seem to suit the purpose of mitigating the existing defects in base material, also assuming that some of those defects have been responsible for the failure.

The grain boundary cracks along Al-Cu-Fe rich precipitates have been found in partially melted zone (PMZ) of heat affected zone (HAZ) of the base material, similar to that is observed in locations away from the weld area (i.e. pure base material). Introduction of welding has come up with problem of more frequent occurrence of cracking in the heat-affected zone (HAZ) of the base material than that at away from it (i.e. pure base material). Grain boundary rich in Al-Fe-Mn precipitates and frequent cracking along the grain boundaries has been observed in weld regions both in longitudinal as well as transverse welds.

Thus, in the post-weld condition and during service of the towing arm, cracks seem to have been present along Al-Cu-Fe and Al-Fe-Mn-rich grain boundaries, respectively at the HAZ and weld regions.

4.3 Various Weld Crack Types

There may be usually two types of cracking in aluminium welds – (i) hydrogen induced cracking (HIC) and/or stress corrosion cracking (SCC) and (ii) hot cracking [11,13,18,19]. In the present scenario, based on fractographic evidence and also the background information, possibility of HIC as well as SCC is zilch [13, 19]. Thus, the existing all the types of cracks are basically hot cracks. This is also well supported by the zig-zag crack paths (representative of intergranular cracking) and distinctive fractographs typical of hot cracking [13,18]. Now, broadly the four factors are influencing hot cracking in aluminium welds: (i) chemistry of base material, (ii) chemistry of filler metal, (iii) thermal stress (arising out of shrinkage during solidification) and (iv) mechanical stress (due to joint configuration/restraint) [20-23]. Nonetheless, one has control over the factors (ii), (iii) (even (iii) is somewhat dependent on (ii)) and (iv)), once chemistry of the base material is fixed by the user. Thus, chemistry of the filler material along with the mixture (base + filler material) as well as joint design may be monitored. The present (hot) crack type includes both solidification as well as liquation cracking. The longitudinal crack of importance seen in the weld region (close to the fusion line) on the primary fracture plane and spanning the whole length is a prime example of solidification crack (marked as secondary crack in Fig. 3). Physical attributes of the crack such as high depth, large length and three-dimensional shape indicate it to be the major culprit of the present failure. In other words, the present failure has initiated with this deep and lengthy discontinuity. Similar types of solidification cracks are also seen at weld region (close to the fusion line) along the transverse welds (Fig. 3g). Small solidification crack well within the weld interior has been observed too occasionally (Fig. 3g). Orientation of these cracks has been found to be parallel to the above-mentioned longitudinal solidification crack. On the other hand, close examination of the PMZ of HAZ in base material reveals the presence of numerous grain-boundary cracks (Fig. 10). These are nothing but the liquation cracks. Solidification and liquation cracks at respective weld and HAZ seem to have been often accompanied by the Al-Fe-Mn and Al-Cu-Fe rich grain boundary precipitates and their cracking.

4.4 Selection of Filler Metal/Alloy

Somewhat detailed input on welding filler material is worth mentioning here, as no information related to welding is available to the user as well as to the investigator.

Use of an Al-Si based is quite justifiable and subsequently discussed. The base Al-Cu-Si (or more specifically, Al-Cu) system has a wide range of crack sensitivity with respect to the Cu content [11-13]. Thus, the use of autogenous welding as well as the introduction of filler material of composition similar to the base material is highly risky. This is for the reason that doing so would result in the same or enhanced level of crack sensitivity to the system. Widely popular filler metals of 4xxx (Al-Si based) and 5xxx (Al-Mg based) series are common choices in Al welding. Interestingly, the alloys of 4xxx series help in diluting the ill effect of Cu locally in this regard. Problem of shrinkage related thermal stresses is quite low in this case. On the other hand, filler materials of 5xxx series aggravate the cracking tendency by combined poorly effect of Cu and Mg on the coherency temperature range.

Failure Mechanism

The Sequence of Failure

Schematic diagram consisting of a proposed sequence of events is shown in Fig. 24. This (Fig. 24a) is described with reference to the whole fracture surface presented in Fig. 3h. Longitudinal three-dimensional crack front spanning the whole length of the weld, close to fusion line is formed as a result of residual stresses coming out of joint constraint and/or heat treatment. This has disturbed the integrity of the joint and thus the component at the beginning of its service operation. This crack front has a curved surface area and extends from location at considerable depth to its opening up at the obtained fracture surface. This, later on, moves towards (both upward and downward) transverse directions (marked as inclined arrows) on the presently obtained plane of fracture surface. Advanced stage of its propagation on the fracture plane is indicated by big inclined arrows. On the other hand, material becomes weakened by the presence of liquation cracks in HAZ (indicated by small straight arrows). Thus, these liquation cracks indirectly have assisted in the present failure by easing the crack propagation stage. Similarly, small (longitudinal) and moderately big (transverse) solidification cracks in transverse welds have assisted the current failure by weakening the microstructure. Varying proportions of the final stages of failure are observed in transverse and longitudinal welds. Weld section 1 is proposed to possess the least area fraction of the final stage of failure. This is due to the consumption of its greater amount by the above said three-dimensional solidification crack front. This is much commensurate with the visual examination (Fig. 3) as well as with the fractographic evidence (Figs. 5 and 7).

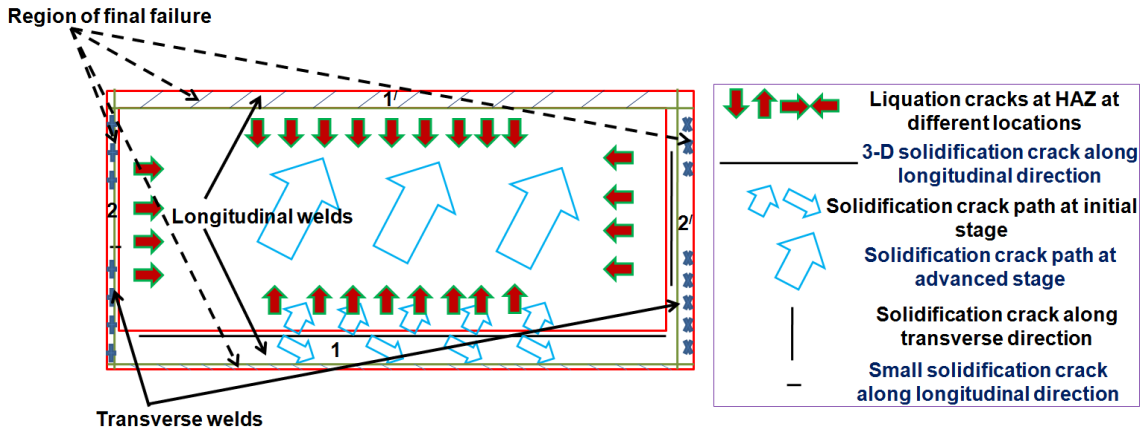

Figure 24: Schematic diagram showing a proposed sequence of events leading to failure

Contribution of Joint Design, System and/or Service Stresses [13, 18, 20-23]

There is absence of uniform weld thickness along the four sides of the failed surface, as mentioned earlier. This may have led to the unequal distribution of the system and/or service stresses and thus aggravating the early likelihood of the failure.

Surrounding fixtures during welding operation has an effect in the present case of weld cracking. Solidification cracks have been observed at welds close to the fusion lines at both the longitudinal as well as the transverse sides. Small solidification cracks aligned along the major axis (i.e., along the longitudinal side on the fracture plane) are also observed within the weld. It is quite clear from the results reported so far, that there has been a dominance of transverse stress over its longitudinal counterpart, as is supported by the frequent occurrence of (solidification) cracks of considerable depth and length, aligned along the longitudinal side. The proposed schematic also corroborates the same in the primary fracture plane which is formed by the movement of longitudinal solidification crack front towards the transverse direction only (Fig. 24).

It is also possible that the residual longitudinal and transverse stresses may be present. This may well come from the joint configuration and/or heat treatment of the component after welding.

Contribution from Service Stress

Failure extending towards the side (transverse) weld zones has exhibited cleavage type of brittle fracture during final stage of failure. This is purely a result of overload. The signature of other types of load is not observed. Presence of cleavage during last stage of failure in both transverse as well as longitudinal weld zones (1, 1′, 2 and 2′ in Fig. 24) in spite of presence of weak intergranular regions (causing solidification cracking) indicate the involvement of rapid rate of loading due to very thin weld areas as compared to the remaining regions of the failed surface.

Microstructural Contribution

The inherent weakness of the parent material such as grain boundary cracks, pores, grain fall outs etc. has still been found to be present at failure location (weld zone, HAZ) as well as at location away from the failure (i.e. unaffected parent base material). Thus, the inherent metallurgical weaknesses of the material still prevail and sometimes have

been aggravated subsequent to the welding (as manifested by more frequent occurrence of the above defects). Thus, the T6 condition of the component material in parent state as well as in as-weld condition does not appear to suit for the present component.

A three-dimensional weld solidification cracking has been found to be the primarily responsible for the creation of primary fracture plane in the present failure. This is also supported by the existence of secondary cracks in the weld zone having trajectory and orientation similar to the fracture path, as mentioned above. Grain boundary cracks at the HAZ (often typified by grain fallout) arising out of the liquation cracking have assisted the present failure. Solidification and liquation cracking have been found to be accompanied with grain-boundary precipitates rich in Al-Cu-Fe and Al-Fe-Mn at the weld and HAZ, respectively.

Longitudinal weld side in the final failure reveals the presence of cleavage signs with occasional occurrence of cleaved facets within the moderately well revealed predominantly intergranular fracture (Figs. 5 and 7). On the other hand, clear disclosure of the cleavage signature along with cleaved facets and faintly revealed two-dimensional intergranular channels have been noticed on the transverse weld side during the final stage of failure. Thus, predominance of traits of cleavage fracture has been noticed especially along the transverse welds unlike along the longitudinal welds. Interestingly, this phenomenon indicates that the Al-Fe-Mn rich precipitates along the grain boundaries in weld region are not so week so as to lead a completely intergranular fracture (as in transverse welds), unless there is a co-existence of solidification cracks along with those precipitates (as in longitudinal welds). The longitudinal weld (weld section 1 in Fig. 24) is thin enough during final stage of failure. This has resulted in non-revelation of cleavage (type of signature of the overload) failure. This low thickness of the final zone of failure is due to the presence of the deep solidification crack of three-dimensional nature extending towards longitudinal weld periphery of the fracture surface at the component edge.

Thus, it is noteworthy from the ongoing discussion so far that precipitates located in base material and HAZ as well as rich in Al-Cu-Fe are possibly relatively softer than those in weld zone and rich in Al-Fe-Mn. This results in the more active participation of Al-Cu-Fe along with the liquation cracking in aggravating the present failure than that of the Al-Fe-Mn along with the solidification cracking phenomenon.

5 CONCLUSIONS

5.1 Towing Arm

1. The present failure appears to have occurred by cracking of the weld region of the towing arm fork, as a result of introduction of weld repairing process as a method of healing of prior existing defects and/or failure at the location of weld area.
2. Primary reason of the weld cracking and failure is the existence of solidification cracks at weld region close to the fusion line (HAZ-weld interface), while liquation cracks at partially melted zone (PMZ) in heat affected zone (HAZ) has contributed to it secondarily by weakening the overall microstructure.
3. Grain boundary precipitates of Al-Cu-Fe type have facilitated development of the liquation cracking, while grain boundary precipitates of Al-Fe-Mn type seem to have resisted the intergranular failure in solidification cracking, under the combined actions of welding induced stresses and service stresses.
4. Improper material processing has led to the weakening of the microstructure of the base material by introduction of pores, grain fall out, thick Al-Cu-Fe type of continuous grain-boundary precipitates and cracking.
5. Weld repairing appears to be not successful at all on the Al-Cu-Si system in the present condition; rather it has aggravated the previously existing improper material condition.

5.2 Towing Pin

Mild (low carbon) steel with low strength level could not bear with the load of the fractured assembly of the towing arm and thus got bent. Its failure is of secondary nature and importance with respect to the failure of towing arm fork and the whole assembly.

6 RECOMMENDATIONS

1. **Material Related:** Pre-existing (casting related) defects such as porosity, grain fall-outs need to be optimized and to be guided by well-defined specification.
2. **Repair Welding Related:** The repair welding, if unavoidable, should be practised with the following precautions.
3. **Process Related:** Process should be monitored based on internationally popular standards for aeronautical applications such as AMS 2175 and AMS-A-21180 [11, 14-17, 19, 24, 25].
4. **Minimization of Residual Stress and Associated Cracking:** Joint design and fixturing should be such that there would be insufficient amount of residual stresses both in longitudinal as well as transverse directions so as not to crack the weld afterwards. Post weld heat treatment (PWHT) may be employed to minimize the ill effect of residual stresses [18, 19, 20-23, 25].

ACKNOWLEDGEMENTS

The authors would like to thank Dr G. Madhusudhan Reddy, Director, DMRL for his constant encouragement to work on the present field. Also, funding from DRDO is gratefully acknowledged.

REFERENCES

1. Part 66 Cat. B1 Module 7 Maintenance Practices, Volume 2, Vilnius-2017, Kazimieras Simonavicius University, https://ksu.lt/wp-content/uploads/2017/06/M7-vol-2-Selected-pages-Maintenance-Practices-2.pdf, Accessed: 15.11.2021.
2. Aircraft incident investigation, http://www.gpiaa.gov.pt/wwwbase/wwwinclude/ficheiro.aspx?access=1&id=9936, Accessed: 15.11.2021.
3. Wen, S., Hui, C., Fu-hai, L., Analysis of Boeing 737 aircraft towing accidents. Engineering Failure Analysis, 2017(80), 234-240.
4. Goglia., J., Two-Hour Delay Follows Tow Bar Break At BOS, https://www.aviationpros.com/gse/pushbacks-tractors-utility-vehicles/tow-bars/blog/10963025/twohour-delay-follows-tow-bar-break-at-bos, Accessed: 20.09.2020.
5. ASTM B26/B26M – 09: Standard Specification for Aluminium-Alloy Sand Castings.
6. Engineering Handbook, Box 232, Exit 49, G. L. Huyett Expy, Minneapolis, KS 67467.
7. Pa, X. M., Brody, H. D., Morral, J. E., 2005. An assessment of thermodynamic data for the liquid phase in the Al-rich corner of the Al-Cu-Si system and its application to the solidification of a 319 alloy. J. Phase Equilibria Diffus. 26, 225-233.
8. Ponweiser, N., Richter, K.W., 2012. New investigation of phase equilibria in the system Al-Cu-Si. J. alloys Compd. 512, 252-263.
9. Kosak, W.E., Cast aluminium rear subframe control arm articulations, U.S. Patent 6648351, 2003.
10. Kosak, W.E., Cast aluminium vehicle subframe with tension/compression struts, U.S. Patent 6742808, 2004.
11. http://www.alcotec.com/us/en/education/knowledge/techknowledge/trouble-shooting-for-aluminium-welding.cfm, Accessed: 15.11.2021.
12. Rakesh, M., Kumar, T.R. Comparative Study of Different Filler Materials on Aluminium Alloys using TIG Welding, International Journal of Engineering Research & Technology (IJERT) ISSN: 2278-0181, 8(8), 2019.
13. Deekhunthod, R. Weld Quality in Aluminium Alloys, https://www.diva-portal.org/smash/get/diva2:724173/FULLTEXT01.pdf, Accessed: 15.11.2021.
14. Esposito, L., Bertocco, A., Cricrì, G., Rosiello, V. Welding-repair effect on F357-T6 aluminium castings: analysis of fatigue life, 2019, The International Journal of Advanced Manufacturing Technology 102(9-12).
15. Using in-process welding to repair aluminium castings, https://www.castingsource.com/articles/using-process-welding-repair-aluminium-castings, Accessed: 15.11.2021.
16. Katsas, S., Nikolaou, J., Papadimitriou, G. D. Microstructural changes accompanying repair welding in 5xxx aluminium alloys and their effect on the mechanical properties, 2006, Materials and Design 27(10), 968-975.
17. Shankar, K., Wu, W. Effect of welding and weld repair on crack propagation behaviour in aluminium alloy 5083 plates, 2002, Materials and Design 23(2):201-208.
18. [18]http://www.adhocmarinedesigns.co.uk/wp-content/uploads/2012/07/ProBoat-June-July-2012-Aluminium-Welds.pdf, last accessed on 15.11.2021.
19. Davis, J.R., Alloying: Understanding the Basics, ASM International, 2001, 351-416, doi:10.1361/autb2001p351, Accessed: 15.11.2021.
20. Withers, P. J., Residual Stress and Its Role in Failure, 2007, Reports on Progress in Physics 70(12):2211, doi:10.1088/0034-4885/70/12/R04.
21. Sun, J., Hensel J., Nitschke-Pagel, T. and Dilger, K., Influence of Restraint Conditions on Welding Residual Stresses in H-Type Cracking Test Specimens, Materials 2019, 12, 2700; doi:10.3390/ma12172700.
22. Luo, Y., Gu, W., Peng, W., Jin, Q., Qin, Q., Yi, C. A Study on Microstructure, Residual Stresses and Stress Corrosion Cracking of Repair Welding on 304 Stainless Steel: Part I-Effects of Heat Input, Materials 2020, 13, 2416; doi:10.3390/ma13102416.
23. De, A., Deb Roy, T., A perspective on residual stresses in welding, Science and Technology of Welding and Joining 2011 16(3), 204-208.
24. How to Avoid Cracking in Aluminium Alloys, https://www.esabna.com/us/en/education/blog/how-to-avoid-cracking-in-aluminium-alloys.cfm#:~:text=To%20counteract%20cracking%20problems%2C%20use,the%20hot%20cracking%20temperature%20range, Accessed: 15.11.2021.
25. The Repair of Aluminium Structures, http://www.alcotec.com/us/en/education/knowledge/techknowledge/the-repair-of-aluminium-structures.cfm, last accessed on 15.11.2021.